SwRI-8972/5

(2)

STUDY OF THE INFLUENCE OF METALLURGICAL FACTORS ON FATIGUE AND FRACTURE OF AEROSPACE STRUCTURAL MATERIALS

By
James Lankford
David L. Davidson
Kwai S. Chan
Gerald R. Leverant

AFOSR FINAL REPORT

This research was sponsored by the Air Force Office of Scientific Research,
Electronic and Materials Sciences Directorate
Under Contract F49620-86-C-0024

Approved for release; distribution unlimited

March 1989

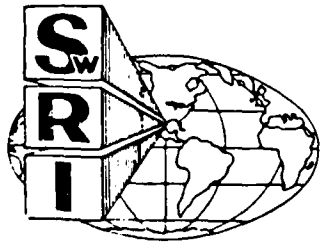

SOUTHWEST RESEARCH INSTITUTE
SAN ANTONIO HOUSTON

SOUTHWEST RESEARCH INSTITUTE
Post Office Drawer 28510, 6220 Culebra Road
San Antonio, Texas 78284

STUDY OF THE INFLUENCE OF METALLURGICAL FACTORS ON FATIGUE AND FRACTURE OF AEROSPACE STRUCTURAL MATERIALS

By
James Lankford
David L. Davidson
Kwai S. Chan
Gerald R. Leverant

AFOSR FINAL REPORT

This research was sponsored by the Air Force Office of Scientific Research,
Electronic and Materials Sciences Directorate
Under Contract F49620-86-C-0024

Approved for release; distribution unlimited

March 1989

Approved:

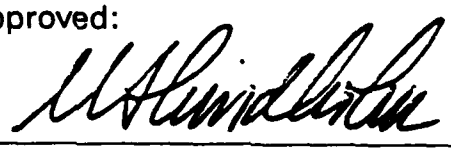

Ulric S. Lindholm, Vice President
Engineering and Materials Sciences Division

TABLE OF CONTENTS

LIST OF ILLUSTRATIONS

LIST OF ILLUSTRATIONS (CONTINUED)

I. CRACK TIP MICROMECHANICS AND FATIGUE LIFETIME PREDICTION

Fatigue cracks grow through a structure because of applied cyclic loads; these loads are the driving force for crack growth, and the crack extends as the response of the material to those loads. Research on this contract in previous years concentrated on deriving an understanding of the crack extension process; therefore, the events attending crack growth were carefully observed under high resolution, dynamic conditions and extensively analyzed. This work revealed that fatigue cracks extend by the same mechanism independent of whether they are small ($5 <$ length < 1000 μm) or large, and independent of the type of cyclic loading to which they are subjected (e.g., constant or variable amplitude), although the details of how the crack extends, and the effects of microstructure, are still too unclear to allow prediction of fatigue crack growth rates.

These observations of similarity in crack growth mechanisms indicated that a shift in the thrust of the research was warranted. Thus, during the last three years, the time covered by this report, the research program has concentrated on determining the magnitude of the local driving force for fatigue crack growth.

Local driving force is the translation of the externally applied (macroscopic) loading to the crack tip (microscopic) region, and as such must include crack closure. Numerous mechanisms have been postulated for crack closure, those considered most applicable to metallic alloys being closure induced by fracture surface oxides and roughness, and plasticity ahead of and behind the crack tip. Despite research during the 20 years since closure was discovered by Elber, quantitative theoretical models for these various mechanisms have not been developed. The exception to this is the work of Newman [1] on plasticity induced closure, and there are differences between what that model predicts and experimental findings [2]. Thus, our work has taken two thrusts: (1) further work on crack closure mechanisms - concentrating specifically on plasticity induced crack closure - and (2) determination of the crack driving force from measured micromechanics parameters, which also indirectly include the effects of closure.

Local driving forces for small and large fatigue cracks subjected to constant amplitude loading were determined for several aluminum alloys and one titanium aluminide alloy. Complex load spectra were simplified by

considering only isolated, single overloads and an over/underload combination. Crack tip opening displacements and strains were measured using the stereoimaging technique for each of these loading conditions and alloys, and the driving force was determined by computation of an equivalent stress intensity factor ΔK_{eq} through use of the cyclic J integral ΔJ using the relation [3]

$$\Delta K_{eq}^2 = E\Delta J = E\Delta\sigma\delta_c \qquad (1)$$

where E = Young's modulus, $\Delta\sigma$ = stress range at the crack tip, and δ_c = crack tip opening displacement. The crack tip stress range was computed by converting crack tip strains (determined with stereoimaging) to stress using the cyclic stress-strain relation. Crack tip opening displacement δ_c was determined from measurements of crack opening displacment as a function of distance behind the crack tip.

Local measurements of fatigue crack closure were made by directly observing the way fatigue cracks open as a function of applied load. These observations were made by using a cyclic loading stage for the scanning electron microscope and determining the point to which the crack had opened as a function of load by stereoimaging. Measurements made using these tools [3,4] have shown that there is a systematic change in effective cyclic stress intensity factor $\Delta K_{eff} = K_{max} - K_{open}$ when the data are plotted as shown in Fig. 1. Data in the figure are shown for R = 0.1, so it is not important whether the absissa is $1/\Delta K$ or $1/K_{max}$, but for large R, all the data fell along the same line when plotted vs $1/K_{max}$ [4]. Mode II opening loads were determined in addition to Mode I opening loads. As the figure indicates, Mode II opening often occurred at a lower load than for Mode I, resulting in a larger value of ΔK_{eff}. The value of this unexpected result increased with decreasing ΔK, so that there is a ΔK_{eff} from Mode II opening at levels of ΔK below which no Mode I opening occurs. If the value of ΔK for which $\Delta K_{eff} = 0$ in Mode I opening is defined as the threshold cyclic stress intensity factor ΔK_{th}, this value (≈ 5.9 MPa$\sqrt{m}$) is larger than that determined from crack growth rate tests (≈ 2 MPa$\sqrt{m}$), but $\Delta K_{eff} \approx 0$ in Mode II at about the same value as was determined from crack growth rate tests.

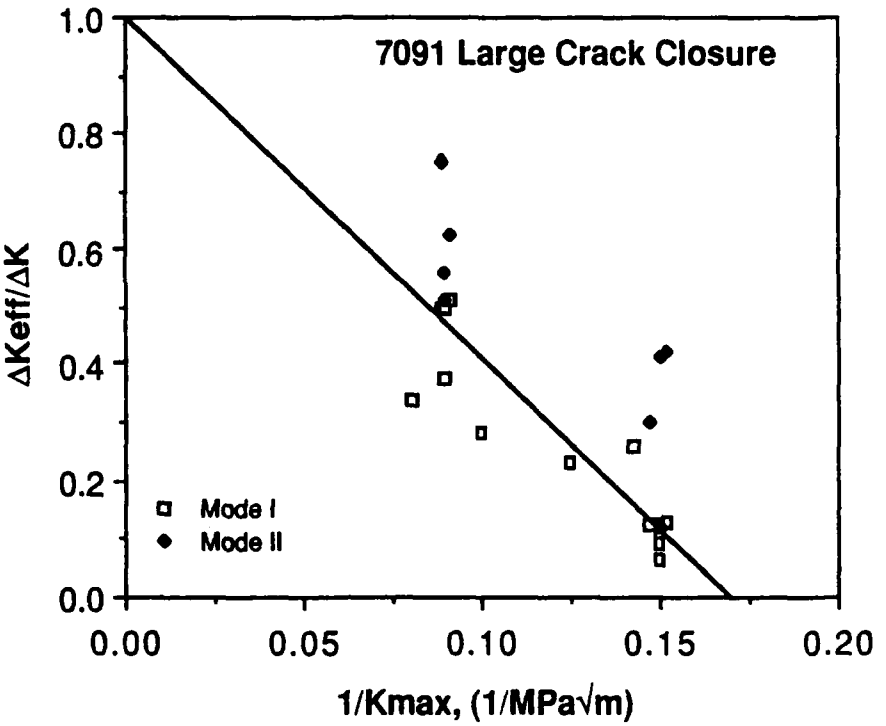

Fig. 1 Fatigue crack closure for the powder metallurgy aluminum alloy 7091, as determined from local measurements of opening load [2]. Note that ΔK_{eff} for Mode II is larger than that for Mode I.

Measurements of Mode I and Mode II crack opening displacements [5] behind fatigue cracks as a function of ΔK agree, in general terms, with the shift toward an increased proportion of Mode II opening with decreasing ΔK. The results shown in Fig. 1 indicate that the driving force for fatigue cracks at $R = 0$ may be written as

$$\Delta K_{eff} = \Delta K - \Delta K_{th} \qquad (2)$$

The expression at $R > 0$ is the same, but with an adjusted value of ΔK_{th} [4].

An explanation for this shift between the dominance of Mode I at large ΔK and Mode II at low ΔK has been sought for some time, and recently, a reason has been suggested [6]. The smooth yield surface of a polycrystalline metal deformed biaxially develops a corner on it when the number of deforming grains is decreased. This corner decreases the resistance of the material to shear

strains. This behavior is relevant to the fatigue threshold because at that ΔK, the plastic zone is reduced to one or a few grains, depending on grain size, which decreases the resistance of these grains to shear, thereby allowing shear at the crack tip to become a prominent feature. This shear mode of deformation ahead of the crack tip leads to a large component of Mode II in the crack opening displacement.

Another way of examining this concept is to compare local determination of driving force, ΔK_{eq}, as determined using eq. (1), to ΔK. For the 7091 aluminum alloy [6], this is shown in Fig. 2.

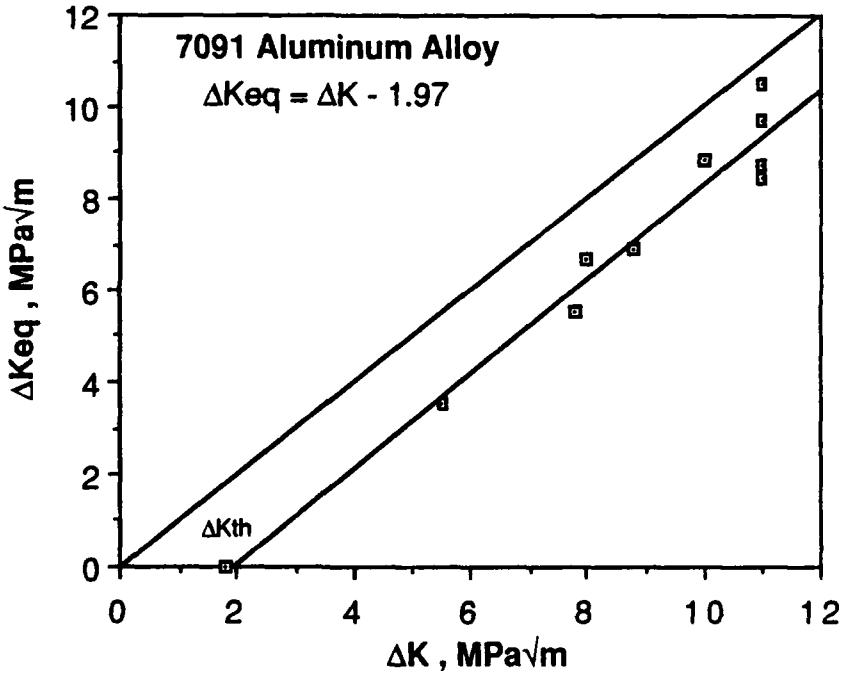

Fig. 2 Comparison of locally determined ΔK_{eq} with applied ΔK, indicating the validity of eq. (2) for describing the crack driving force [7].

Results similar to those shown in Figs. 1 and 2 were obtained also for large fatigue cacks in 7075-T651 aluminum alloy [7], so it appears that eq. (2) has general validity. However, difficulty has been encountered in applying these concepts to the titanium alloys Ti-6Al-4V and CORONA-5. Reasons for this difficulty are not known, but these titanium alloys have significantly different slip characteristics than aluminum alloys. Therefore, the breadth of validity of these concepts must be further explored for other material systems.

Small cracks in 7075 aluminum alloy and in the nickel-based superalloy Astroloy have also been carefully examined. Local crack closure measurements were made and ΔK_{eq} was determined from crack tip parameters, just as for large cracks. The results, however, were completely different. This is illustrated in Fig. 3 for 7075-T651, which compares the closure characteristics of small and large fatigue cracks. The closure level, K_{open}, for small cracks increases in proportion to K_{max}, unlike large cracks.

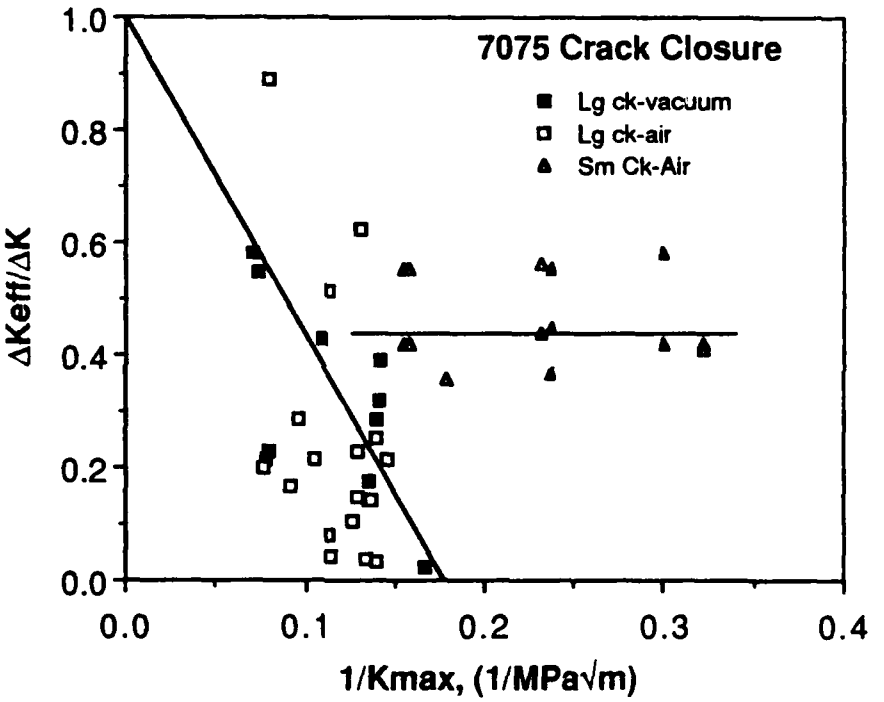

Fig. 3 Comparison of locally measured crack closure data for small and large fatigue cracks in 7075 aluminum alloy.

Also, as for large cracks, crack tip micromechanics parameters were used to determine ΔK_{eq} using eq. (1), and these measurements were compared to the applied ΔK. The results of this comparison are shown in Fig. 4, where it may be seen that there is, in fact, a substantial difference.

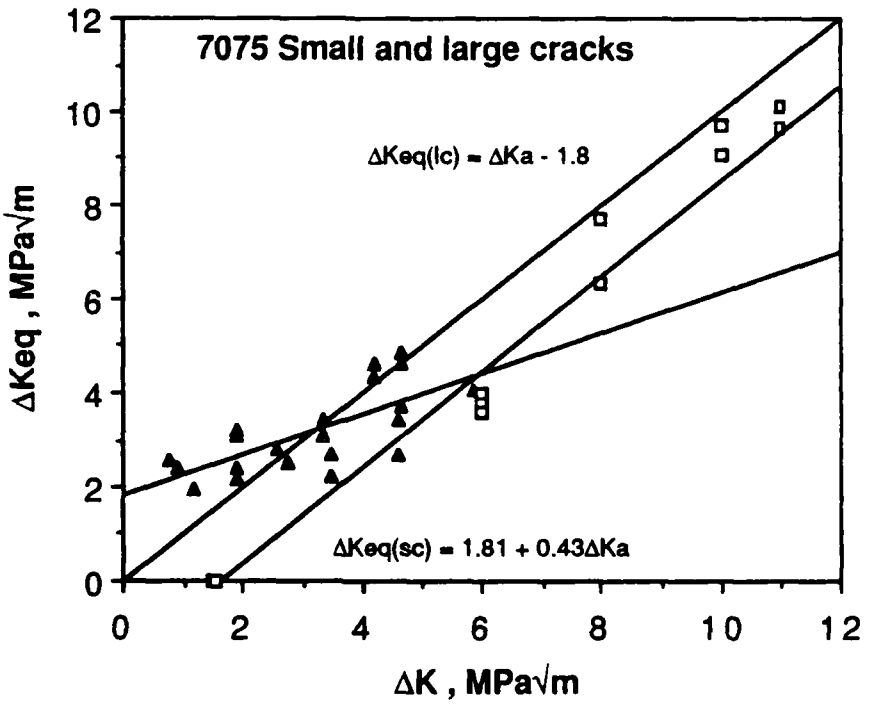

Fig. 4 Comparison between local driving force, ΔK_{eq}, and applied ΔK for small and large fatigue cracks in 7075. Large cracks follow the functional form given by eq. (2) but for small cracks a different relationship is needed.

Another term must be added to the description of driving force for small cracks to account for change in slope. Thus, eq. (2) becomes

$$\Delta K_{eq} = \Delta K_i + \Delta K - \Delta K_c \qquad (3)$$

Since $\Delta K_c = \alpha \Delta K$, as shown in Fig. 3, then eq. (3) may be rewritten as

$$\Delta K_{eq} = \Delta K_i + \beta \Delta K \qquad (4)$$

where $\beta = 1-\alpha$ is the slope of the line in Fig. 4. The term ΔK_i is thought to arise from additional crack tip plasticity which comes from the high level of cross-sectional stress in which these small cracks were growing (80% of yield). Also, this term might account for the differences in constraint experienced between a large crack at low cross-sectional stress and a small crack at high cross-sectional stress. These differences in constraint and

stress level cause the strain distributions between small and large cracks to be different [8], and this allows an estimate of ΔK_i to be made on the basis of the large crack ΔK_{th}, as is more fully explained in [7].

If these concepts of local driving force for small and large fatigue cracks are correct, then it should be possible to correlate crack growth rates on the basis of ΔK_{eff} using eq. (2) or eq. (4). Growth rates for small and large fatigue cracks in 7075 aluminum alloy, the superalloy Astroloy, and the Super Alpha 2 titanium aluminide alloy have been successfully correlated using crack tip micomechanics measurement and the concepts discussed above. Results for 7075 have been published in the open literature [7], but results for Astroloy and Super Alpha 2 are still to be found only in reports. Fig. 5 shows data for Super Alpha 2, together with the functions used to compute ΔK_{eff}.

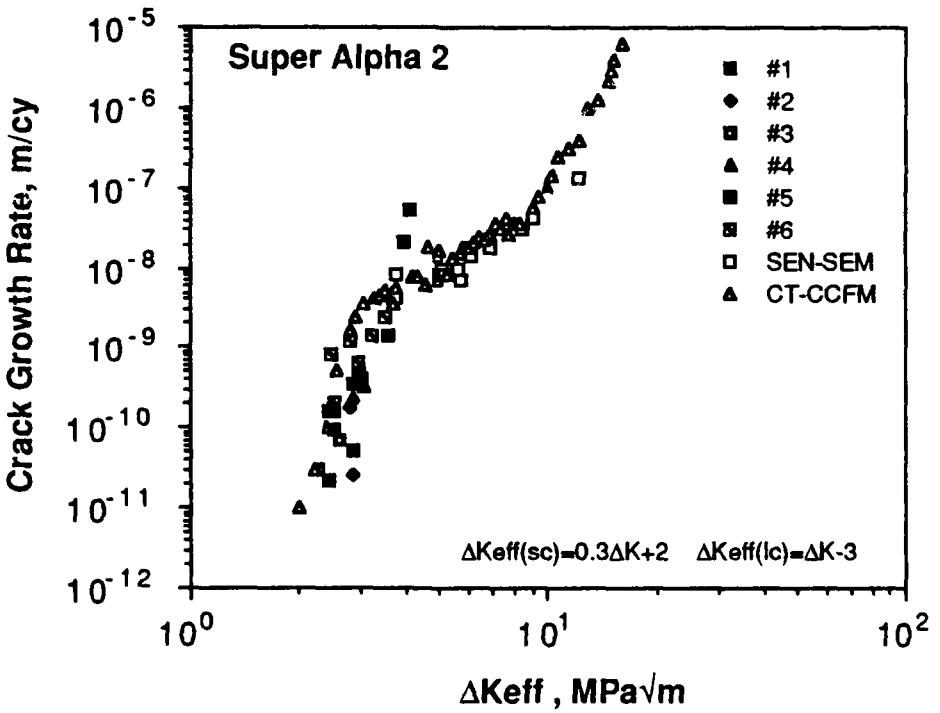

Fig. 5 Correlation between crack growth rates and effective ΔK for small and large fatigue cracks in a titanium aluminide alloy. The large crack data are from single edge notched (SEN) and compact tension (CT) specimens.

For this titanium aluminide alloy, the correlation between small and large crack growth rates is very good. It should be noted that the value of ΔK_i in

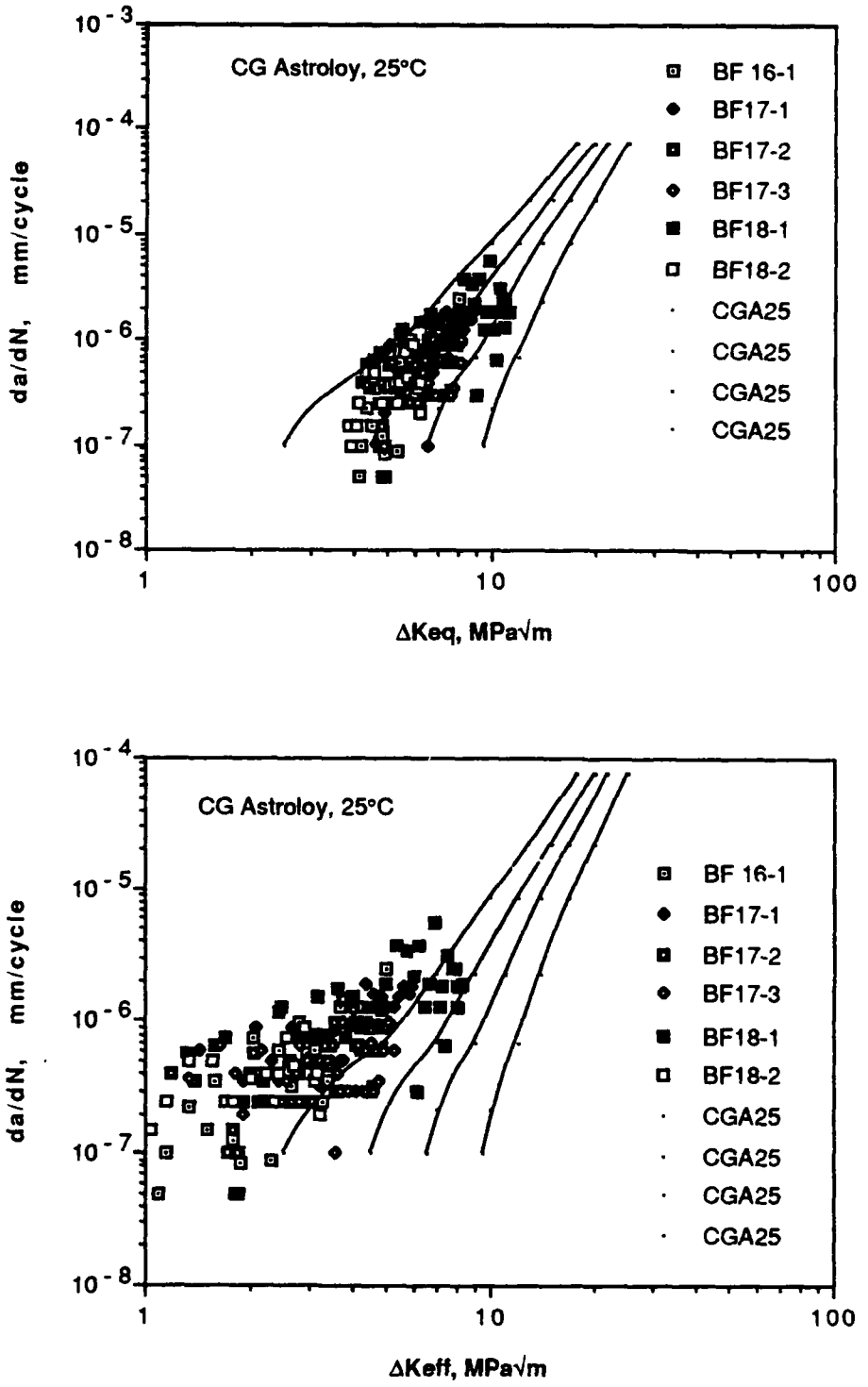

Fig. 6. Crack growth rates for large and small fatigue cracks in coarse grained Astroloy at 25°C showing (upper figure) the effect of correcting the driving force using eq. (4), which includes ΔK_i, compared to using only closure to determine ΔK_{eff} (lower figure).

eq.(4) was determined from the large crack threshold ΔK_{th} using the computational method given in [7].

For Astroloy, there is more uncertainty in the correlation because of differences found in large crack growth data [9]. These results are shown in Fig. 6. The most probable magnitude of ΔK_{th} = 3.5 MPa$\sqrt{m}$, as determined from a survey of available large crack data [9], so the correlation between small and large cracks on the basis given in eq.(4) appears to be applicable for this material also. Note how much better correlation is obtained by including both terms in the description of small crack driving force, Fig. 6(a), rather than using closure alone, Fig. 6(b). Similar results were also found for small cracks grown in coarse and fine grained Astroloy at 600°C and for Waspaloy at 600°C [9].

Since fatigue cracks under variable amplitude loading appear to be growing by the same mechanism as they are under constant amplitude loading, then it may be hypothesized that the reason crack growth rates cannot be predicted from constant amplitude loading must arise from an inability to determine the local crack driving force under variable amplitude loading. To examine this conjecture, the same methods used for determining local driving force for small and large cracks under constant amplitude loading were used for crack growth under variable amplitude loading. The variable amplitude loading sequences used to test this hypothesis were overloads of two different magnitudes at R ≈ 0, and an overload/underload combination for R = 0.5. The results of correlating crack growth rates before and after the overloads and over/underload combination with ΔK_{eff} ($=\Delta K_{eq}$) are shown in Fig. 7.

As the figure indicates, the correlation between crack growth rates under constant amplitude and variable amplitude is much better if the local driving force is used than if only crack closure is used, just as was shown for the correlation between small and large cracks in Astroloy, Fig. 6. Thus, it is apparent that the hypothesis has been verified, and that the problem with determining crack growth rates under variable amplitude loading condtions is that of describing the transfer function between externally applied load and the local crack driving force.

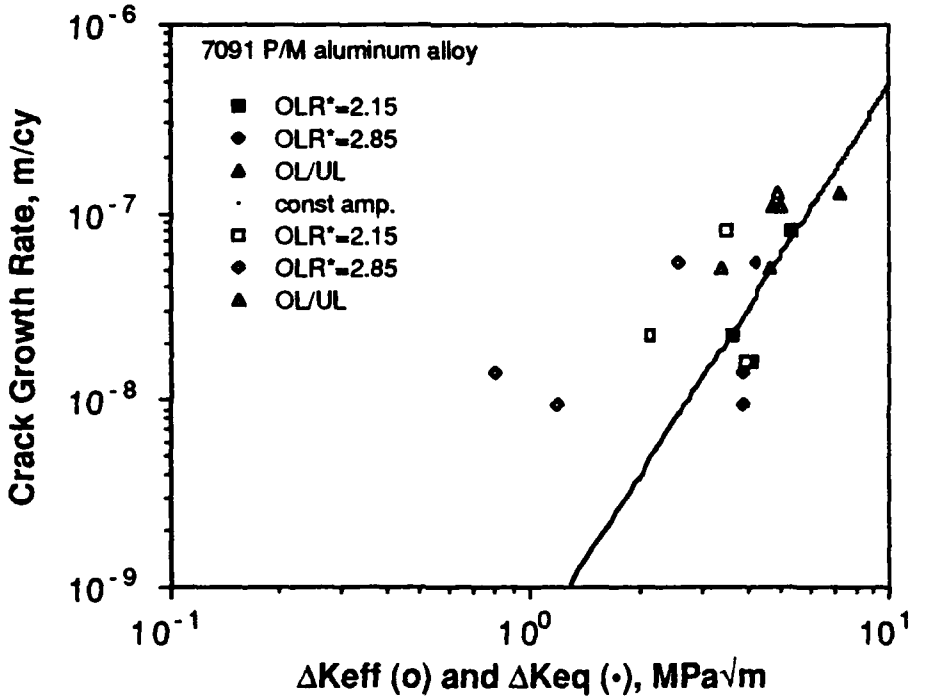

Fig. 7 Correlation between crack growth rates measured during variable amplitude loading and local driving force, as determined from closure only (ΔK_{eff} - open symbols), and also from crack tip micromechanics (ΔK_{eq} - closed symbols) [10]. OLR* gives the magnitude of the overload. The solid line is for constant amplitude loading.

Accomplishments:

1. Measurements of crack closure immediately at the crack tip have shown that there is a systematic variation of the local crack driving force, ΔK_{eff}, over a wide range of ΔK for constant amplitude loading. The Mode I and Mode II levels of crack closure appear to be consistent with measurements of mode mix in crack opening displacements. For large cracks, local driving force can be determined from the relation $\Delta K_{eff} = \Delta K - \Delta K_{th}$.

2. The hypothesis that differences in the correlation between crack growth rates and ΔK for small and large cracks are caused by differences in local crack driving force was tested for aluminum alloys and was verified. Determination of local driving forces for small cracks showed that an additional term was required to describe the relation between local and applied ΔK values, but when

this term was included, crack growth rates for both small and large cracks correlated on the basis of the local driving force.

3. The crack growth rates for large and small cracks in 7075 aluminum alloy, Super Alpha 2 titanium aluminide alloy, and the superalloy Astroloy were correlated by using systematic adjustments in crack driving force.

4. Crack growth rates under variable amplitude loading were found to correlate with constant amplitude loading when local driving forces were measured using crack tip micromechanics.

5. The results of this research, coupled with previous findings, indicate that differences in crack growth rate correlations with ΔK, when cracks are of different sizes, or under variable amplitude loading, are due not to differences in the mechanisms of crack advance, but to inaccuracies in determining the transfer function between computed ΔK and the local crack driving force, ΔK_{eff}.

References:

1. J.C. Newman in **ASTM STP -590**, Am. Soc. Test. Mat., Philadelphia, 1976, pp. 281-301.
2. D.L. Davidson in **ASTM STP - 982**, Am. Soc. Test. Mat., Philadelphia, 1988, pp. 44-61.
3. S.J. Hudak and K.S. Chan in **Small Fatigue Cracks**, TMS-AIME, Warrendale, PA, 1986, pp. 379-406.
4. S.J. Hudak and D.L. Davidson in **ASTM STP - 982**, Am. Soc. Test. Mat., Philadelphia, 1988, pp. 121-138.
5. D.L. Davidson and J. Lankford, *Materials Sci. and Engng.*, v.60, 1983, pp. 225-229.
6. S.J. Harren, Southwest Research Institute, private communication in connection with SwRI project 06-9456, 1988.
7. D.L. Davidson, *Acta Metallurgica*, v.36, 1988, pp. 2275-2282.
8. J. Lankford and D.L. Davidson in **Fatigue Crack Growth Threshold Concepts**, TMS-AIME, Warrendale, PA, 1984, pp. 447-463.
9. S.J. Hudak, D.L. Davidson, K.S. Chan, A.C. Howland, and M.J. Walsch, **AFWAL-TR-88-4090**, June 1988.
10. D.L. Davidson in **Fatigue Crack Growth under Variable Amplitude Loading**, Elsevier, London, 1988, pp. 1-11.

II. MICROSTRUCTURE/PROPERTY RELATIONSHIPS IN ADVANCED STRUCTURAL ALLOYS

A. Research Objectives

1. Develop a fundamental understanding of the fracture mechanisms in dispersoid strengthened Al-Fe-X alloys
2. Identify origins of brittle fracture and low fracture toughness
3. Establish microstructure/fracture toughness relationships
4. Identify means for enhancing the fracture toughness of Al-Fe-X alloys

B. Summary of Research Efforts

Both experimental and theoretical studies were conducted to achieve the program objectives. The experimental efforts involved characterization of microstructure, tensile and fracture properties, crack tip behavior, and fracture mechanisms in dispersion-strengthened aluminum alloys intended for elevated temperature applications up to 316°C. The experimental efforts were augmented by theoretical analyses to establish criteria for brittle-to-ductile fracture transition, origins of brittle fracture and low toughness, thin sheet toughening by crack divider delamination, and the role of interface decohesion in the fracture behavior of Al-Fe-X alloys.

Five Al-Fe-X alloys including Al-8Fe-7Ce, Al-8Fe-2Mo-1V, Al-10.5Fe-2.5V, Al-8Fe-1.4V-1.7Si, and Al-5Cr-2Zr were selected for study. All five alloys were obtained in the form of extruded rectangular bars. The producer, extrusion ratio, and the form of particulates used to make the alloys were reported in [1], together with the size, volume fraction, and type of intermetallic dispersoids in individual alloys [1-3]. Summary of the yield stress, ultimate tensile strength, strain hardening exponent, true fracture strain, fracture toughness (K_{IC}), and tearing modulus, T_R, of the five Al-Fe-X alloys in the LT orientation at 25° and 316°C is presented in Table I. Fracture properties for the TL orientation are presented in [1]. A wide range of K_{IC} and T_R values is observed in these alloys. This range of fracture behavior will be discussed based on the following considerations: (1) fracture mechanisms, (2) origins of brittle fracture and low toughness, (3) effects of delamination on fracture toughness, (4) microstructure/fracture toughness relationships, and (5) toughness enhancement.

TABLE I.

TENSILE AND FRACTURE PROPERTIES OF Al-Fe-X ALLOYS IN THE LT ORIENTATION AT 25° AND 316°C

Material	T, °C	Yield Stress MPa	σ_{uts} MPa	n	Elongation, %	$\varepsilon_f^{\#}$, %	K_{IC} MPa$\sqrt{m}$	Tearing Modulus T_R
Al-8Fe-7Ce	25°C	418.9	484.9	.053	7.0	15	8.5	0.0
	316°C	178.1	193.8	.050	7.6	28	7.9[+]	4.0
Al-8Fe-2Mo-1V	25°C	323.5	406.6	.084	6.7	18	9.0	0.0
	316°C	170.0	187.5	.043	7.2	27	8.1[+]	16.1
Al-10.5Fe-2.5V	25°C	464.1	524.5	.036	4.0	8	5.7	0.0
	316°C	206.3	240.0	.043	6.9	26	8.1[+]	1.3
Al-8Fe-1.4V-1.7Si	25°C	362.5	418.8	.085	6.0	41	32.0[+]	23.2
	316°C	184.4	193.8	.043	8.0	43	14.9[+]	7.4
Al-5Cr-2Zr	25°C	317.2[16]	351.0[16]	.031[16]	11.9[16]	46[*][16]	14.8[+]	33.0

\# Local fracture strain measured using tensile specimens gridded with 0.5 mm diameter circles

\+ Computed from J_{IC} data using the expression: $K_{IC} = [EJ_{IC}/(1-\nu)^2]^{\frac{1}{2}}$

* Computed from reduction in area

1. Fracture Mechanisms in Al-Fe-X Alloys

The fracture mechanisms in the Al-Fe-X alloys at 25 and 316°C were studied by examining fractured tensile and K_{IC} specimens using optical and scanning electron microscopies, as well as by Auger spectroscopy when necessary. The fracture processes which occurred ahead of a growing crack in individual Al-Fe-X alloys were identified by arresting the crack in the J_{IC} specimens, sectioning the unfractured specimens, and examining the crack tip region using either optical or scanning electron microscopy.

Studies of tensile and K_{IC} specimens revealed that fracture in Al-8Fe-7Ce was initiated at small dispersoids located near Zone A particles. The crack path was generally near Zone A particles, though not necessarily along the matrix/Zone A particle interfaces. The Al-Fe-Mo-V alloy contained a small amount of large, extraneous Al-Fe intermetallic particles which initiated fracture in tensile specimens. Fracture of cracked specimens, however, was controlled by void nucleation at small dispersoids. The Al-Fe-V alloy failed by a combination of void nucleation at small dispersoids, delamination along prior powder particle boundaries (PPBs), and powder pull-outs. All three alloys showed identical fracture behavior in both the LT and TL orientations at ambient temperatures.

The fracture mechanisms in the Al-Cr-Zr alloy at 25°C, the Al-Fe-Mo-V alloy at 316°C, and the Al-Fe-V-Si alloy at both temperatures were found to be more complex. Two possible fracture mechanisms were identified in the LT-oriented specimens of these three alloys. The first one involved void nucleation at dispersoids ahead of the crack tip by a localized shear process. This fracture process is illustrated in Figure 1 for the Al-Cr-Zr alloy tested at 25°C. Figures 1(a) and (b) show a crack which propagated along a localized shear band emitted from the crack tip. The shear band contains a number of voids which coalesced and joined with the main crack by localized shear fracture of the ligaments between the voids. Thus, fracture occurred in a manner similar to the classical void sheet mechanism [4], with void nucleation and coalescence taking place by the localized shear process suggested by Clayton and Knott [5]. The failure process ahead of the crack tip was predominantly void nucleation at dispersoids [Figure 1(c)]. Voids were observed at a 45° angle to, and directly ahead, of the crack tip; once nucleated, they quickly coalesced and joined with the main crack.

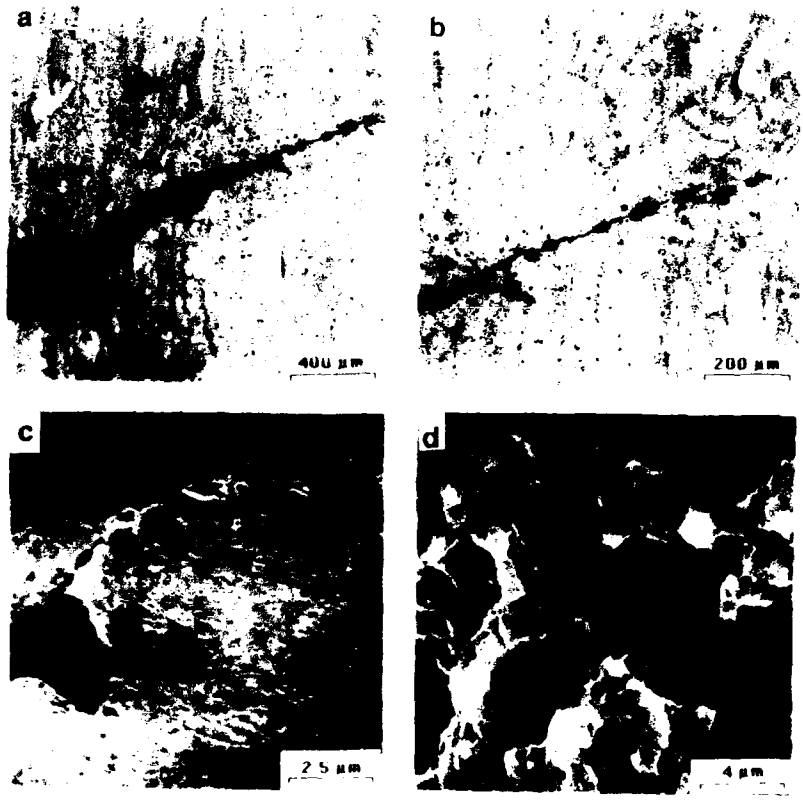

Figure 1. Void nucleation at dispersoids by a localized shear process in the Al-Cr-Zr alloy: (a) and (b) localized shear bands with voids ahead of the crack tip, (c) decohesion of dispersoids ahead of the crack tip, and (d) small dimples observed on the fracture surfaces.

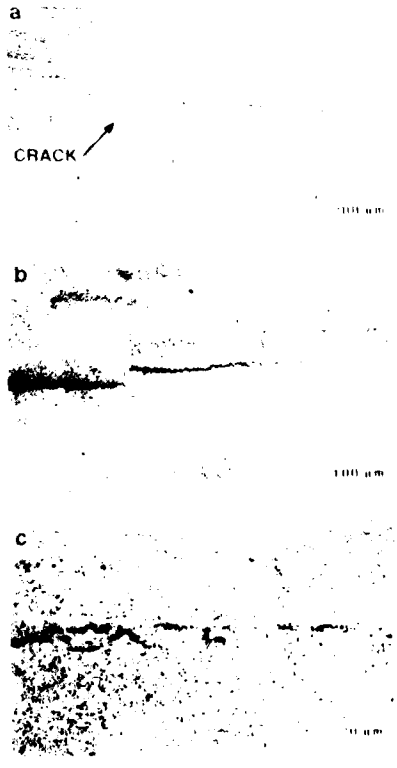

Figure 2. Fracture mechanisms along prior powder-particle boundaries (PPBs): (a) a transverse crack along a PPB, (b) a microcrack located ahead a main crack aligned along a PPB, and (c) voids nucleated ahead of the microcrack.

Consequently, the number of cavities observed was few, and they were relatively difficult to detect. The cavities were generally small, consistent with the small and shallow dimples observed on the fracture surface [Figure 1(d)].

The second fracture process observed was delamination along prior powder-particle boundaries (PPBs). In the LT orientation, most of the extruded prior powder-particle boundaries were aligned parallel to the loading axis. Delamination of PPBs normal to the transverse direction resulted in the formation of microcracks ahead of the main crack. On the other hand, fracture along PPBs normal to the thickness direction resulted in crack divider delamination and thin sheet ligaments in the process zone. The mechanisms for these two delamination processes were found to be essentially identical to those observed in the propagation of a transverse crack along a prior powder-particle boundary. As illustrated in Figure 2, transverse crack growth involves void nucleation by separation of PPBs (presumably at oxide fragments), coalescence of the voids to form microcracks, and their subsequent linkage with the main crack. The essential difference among the three types of PPB delamination which are summarized in Figure 3 (a)-(c), is in the orientation of the PPB with respect to the main crack. In all three cases, delamination occurred at regions of high normal stresses, suggesting that void nucleation at oxide fragments along PPBs was controlled by a normal stress process. In contrast, void nucleation at dispersoids was controlled by a localized shear process, which is illustrated in Figure 3(d). Since high normal stresses are readily available ahead of a crack tip, void nucleation at oxide fragments is relatively easy compared to void nucleation at dispersoids.

2. Origins of Brittle Fracture and Low Fracture Toughness

Origins of low fracture toughness in Al-Fe-X alloys were examined from both microstructural and micromechanical considerations. Microstructurally, the sources of low fracture toughness in Al-Fe-X alloys were identified to be relatively easy void nucleation at oxide fragments along PPBs, and also at dispersoids with incoherent interfaces. Void nucleation at oxide fragments was relatively easy because it appeared to be controlled by a normal tensile stress process, which could be readily attained ahead of a crack tip and occurred with little plastic deformation. On the other hand, a localized shear process was needed in order to induce void nucleation at dispersoids by slip impingement. This process required plastic

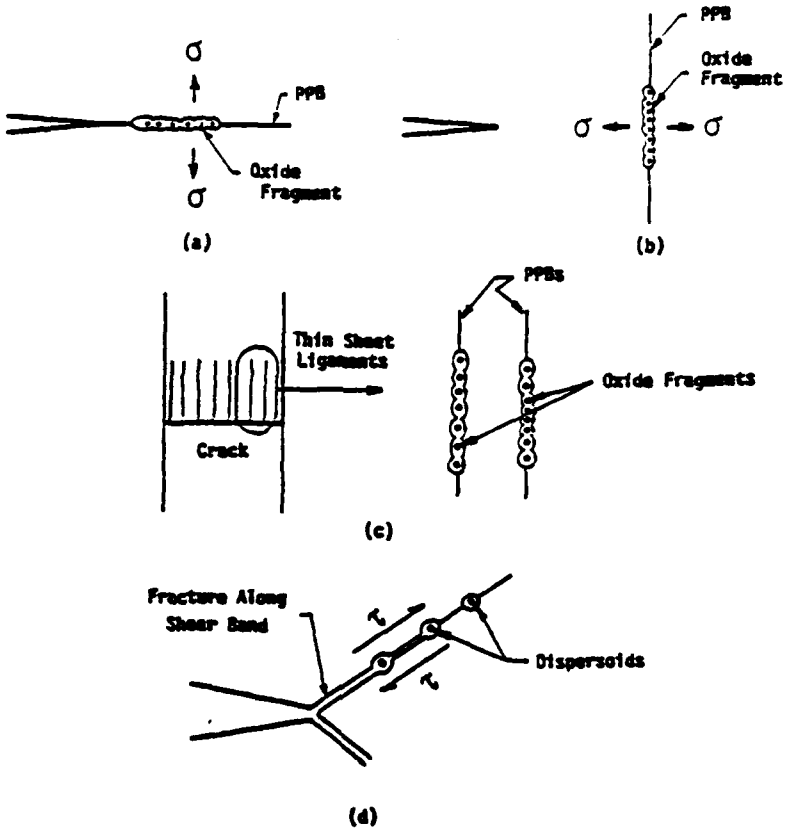

Figure 3. Summary of fracture mechanisms in the Al-Fe-X alloys: (a) - (c) void nucleation at oxide fragments clustered along PPBs by a normal stress process, and (d) void nucleation at dispersoids by a shear process. Note that crack divide delamination in (c) leads to thin sheet toughening, while the delamination processes depicted in (a) and (b) lead to lowering of fracture resistance.

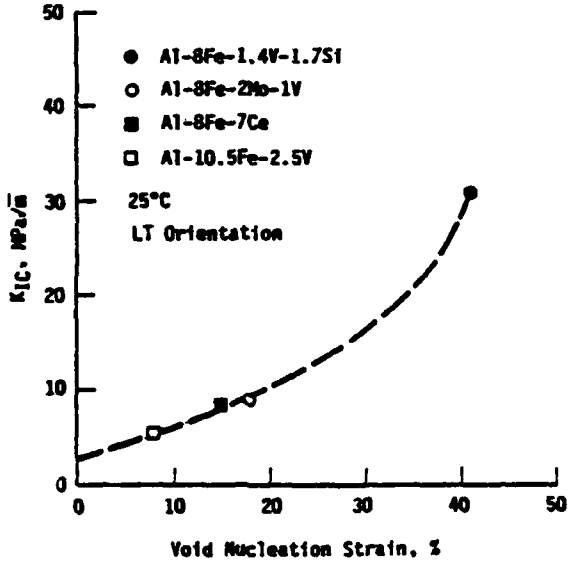

Figure 4. Dependence of crack initiation toughness, K_{IC}, on void nucleation strain in Al-Fe-X alloys at 25°C.

work, and therefore led to a higher fracture toughness when a substantial amount of plastic work was expended prior to shear localization. The fracture toughness of Al-Fe-V-Si, Al-Cr-Zr, and Al-Fe-Mo-V alloys in the TL orientation is lower than those in the LT orientation; this is because of the differences in the void nucleation processes. In contrast, variation in fracture toughness among alloys tested in the LT orientation was due to differences in the void nucleation strain, which appeared to depend on the coherency of the matrix/dispersoid interface. Unlike conventional aluminum alloys, void growth does not appear to be important in the Al-Fe-X alloys because the voids, once nucleated, quickly coalesce either to link with the main crack, or to form microcracks which subsequently join with the main crack. The highest void nucleation strain was observed in the Al-Fe-V-Si alloy, which contained small, spherical cubic silicides whose interfaces are coherent with the matrix. Dispersoids in the Al-Fe-V, Al-Fe-Ce, and Al-Fe-Mo-V alloys are generally larger, noncubic, and incoherent with the matrix. The nucleation strains for these alloys were found to be lower. Figure 4 shows that the K_{IC} values of Al-Fe-X alloys at 25°C increase with increasing void nucleation strain.

Al-Fe-X alloys were found to exhibit a brittle-to-ductile fracture transition, despite the fact that fracture occurred by a microvoid process. This is in contrast to classical brittle-to-ductile fracture phenomena, which usually involve a change of fracture mechanism from cleavage to ductile void growth. Since a change in fracture mechanism does not occur, brittle-to-ductile fracture in Al-Fe-X alloys is best described in terms of the tearing modulus, T_R, which is a normalized parameter representing the tearing resistance of a material. The brittle-to-ductile fracture transition observed in Al-Fe-X alloys was analyzed by considering the critical condition which would lead to crack instability after an incremental extension [6]. The analysis indicated that the experimental tearing modulus is the consequence of the competition between the intrinsic tearing resistance and the tearing term induced by crack extension, both of which were expressed in terms of the normalized parameter, $\Omega = E\varepsilon_{1f}/\sigma_o$, where E is the elastic modulus, ε_{1f} is the true fracture strain, and σ_o is the flow stress. The analysis led to a general expression for predicting the tearing modulus of a structural material based on the elastic modulus, true fracture strain, and flow stress. Comparison of the predicted tearing modulus with results of Al-Fe-X alloys from this program and those of conventional Al-alloys [7], and Al-Li alloys [8,9] from the literature, is shown in Figure 5. A more extensive comparison of the model with experimental data for steels, Ni-, Al-, and Ti-alloys is presented in Ref. 6.

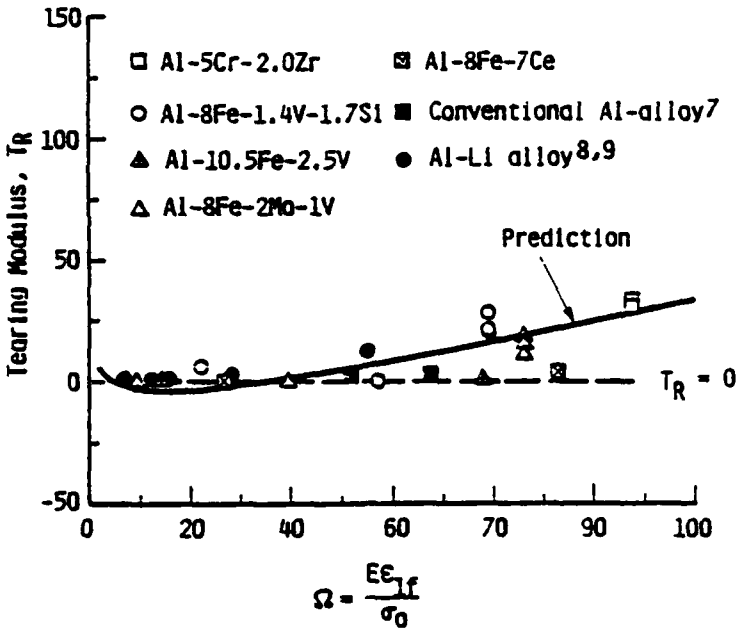

Figure 5. Tearing moduli, T_R, of Al-Fe-X, conventional Al-, and Al-Li alloys compared with model prediction.

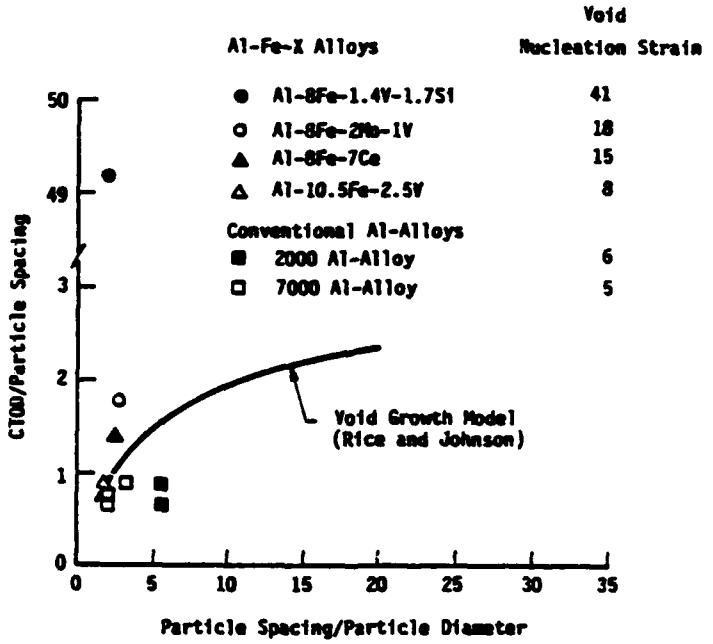

Figure 6. Comparison of the CTODs at fracture of Al-Fe-X alloys with the void growth model of Rice and Johnson.

The crack growth analysis revealed that Ω must exceed 34.5 in order for $T_R > 0$, i.e., for ductile fracture to occur. Moreover, since Ω depends on ε_{if}, an intrinsic fracture strain must be exceeded in order to attain stable crack growth and ductile fracture. The theoretical prediction was verified by comparing the predicted brittle-to-ductile fracture transition boundary with experimental data for a number of structural materials including Al-Fe-X alloys. It also was verified by crack tip strain measurements obtained using the stereoimaging technique [10,11]. These results revealed the dominance of the HRR field (1/r singularity) for a stationary crack, the dominance of the logarithmic singularity for a growing crack, and that a critical fracture strain must be exceeded in order to cause sufficient nonproportional loading within the process zone to cause the transition of the HRR singularity to the logarithmic singularity. Thus, brittle fracture in some of the Al-Fe-X alloys can be attributed to an insufficient intrinsic ductility altering the 1/r singularity of a stationary crack to the less singular growing crack (logarithmic) singularity. This, from micromechanical considerations, is the origin of brittle fracture in Al-Fe-X alloys. The lack of intrinsic ductility in some of the Al-Fe-X alloys originates from microstructural factors, i.e., coherency of dispersoid/matrix interface, and void nucleation at oxide fragments and dispersoids, as discussed earlier.

3. Effects of Delamination on Fracture Toughness

Delamination along PPBs resulted in the formation of thin sheet ligaments in the fracture process zone in some of the Al-Fe-X alloys studied, including the Al-Fe-V-Si and Al-Cr-Zr alloys. The thin sheet ligaments were arranged in a crack divider configuration with internal free surfaces between individual ligaments. As a result, triaxial stresses within the process zone were relaxed, and the critical fracture strain and toughness were increased because of reduction of mean stresses with the process zone. This type of toughness enhancement, which has also been observed in Al-Li alloys at cryogenic temperatures [12,13], has been referred to as "thin sheet toughening" [3] or "crack divider delamination toughening" [13].

The premise of the thin sheet toughening mechanism is that the fracture toughness of a thick component or a plane strain specimen should be controlled by the fracture properties of individual ligaments after it has delaminated. Therefore, the K_C value of an alloy which exhibits thin sheet toughening is expected to be independent of specimen thickness. In contrast,

an alloy which does not exhibit crack divider delamination and thin sheet toughening is expected to show an increase in K_C with a reduction of specimen thickness. The notion that thin sheet toughening was present in Al-8Fe-1.4V-1.7Si was tested by measuring K_C as a function of specimen thickness [1]. The K_C of Al-Fe-V-Si was found to be independent of thickness, while that for Al-8Fe-2Mo-1V, which did not exhibit crack divider delamination, increased with decreasing thickness. The result confirmed that the fracture toughness of thick specimens of the Al-Fe-V-Si alloy was controlled by individual thin sheet ligaments, as postulated in the thin sheet toughening mechanism.

Delamination of PPBs located directly ahead of the crack tip resulted in microcracks which were aligned parallel to the extrusion direction. The microcracks were generally antishielding since they increased the local K of the main crack. The microcracks propagated in an unstable manner once the local K values at their tips exceeded the K_{IC} value for the TL-orientation, because of a zero value for the tearing modulus for that direction. This type of delamination led to fracture anisotropy and an unusual fracture behavior in some of the Al-Fe-X alloys, as discussed in detail in Ref. 1.

4. Microstructure/Fracture Toughness Relationships

The prevailing view as to the critical process which controls fracture toughness in most engineering alloys, including conventional aluminum ones, is void growth ahead of the crack tip. This view has been established on the basis of extensive experimental observations which indicate that void nucleation is relatively easy (at ≈ 5% plastic strain for conventional Al-alloys [14]) in most engineering alloys. The most oft-referenced relation between fracture toughness and microstructure (particle spacing and size) is that of Rice and Johnson [15], which is a void growth model that relates the critical CTOD at crack initiation to the particle spacing. Comparison of the Rice and Johnson void growth model with experimental data of Al-Fe-X and conventional Al-alloys [14] is shown in Figure 6. The important point in this figure is that the void growth model is adequate in predicting the critical CTOD in terms of the particle spacing for conventional Al-alloys, for which the void nucleation strain is small, but substantial discrepancies between model and experiment were observed for the Al-Fe-X alloys, for which the void nucleation strain is larger. This is not a surprising result, since the controlling fracture mechanism in Al-Fe-X alloys is, as indicated earlier, void nucleation, a

process which was not considered in the Rice and Johnson model. For the Al-Fe-X alloys studied, the ratios of dispersoid spacing to dispersoid diameter are essentially equivalent, but the critical CTOD varies greatly because of differences in the void nucleation strain. The implications of the results in Figure 6 are: (1) increasing the void nucleation strain is a viable means for increasing fracture toughness; (2) the void nucleation process must be considered in modeling fracture toughness of Al-Fe-X alloys; (3) fracture toughness is not related solely to the ratio of particle spacing to particle size.

An alternative means to establishing microstructure/property relationship is to relate fracture toughness (K_{IC}) to tensile properties. Such a relation must include void nucleation, as it is an important part of the fracture process in Al-Fe-X alloys. A fundamental relation does not exist currently. However, a semi-empirical relation was developed to describe the K_{IC} value for Al-Fe-X alloys under plane strain fracture and for fracture with thin sheet toughening effects [3]. In this model, K_{IC} is proportional to $n\sqrt{E\sigma_y\varepsilon_{1f}}$, where n is the strain hardening exponent, E is Young's modulus, σ_y is the yield stress, and ε_{1f} is the true local fracture strain including contributions from void nucleation, growth, and coalescence. The model is based on the assumption that fracture occurs when the effective strain, $\bar{\varepsilon}$, within the process zone reaches a critical value, $\bar{\varepsilon}^*$, which decreases with increasing triaxial stresses. Empiricism in the model arises because knowledge of the size of the process zone is required; this cannot be predicted at the present time, but must be inferred from experimental data. Figure 7 shows correlation of the model and plane strain fracture toughness data for Al-Fe-X alloys.

The model was used to estimate the maximum effects of thin sheet toughening on fracture toughness enhancement. Since delamination in Al-Fe-X alloys results in thin sheet ligaments free from normal stresses, crack extension across these ligaments occurs under the plane stress condition, as opposed to the plane strain condition which would prevail had delamination not occurred. The relaxation of triaxail stresses in the crack tip process zone would lead to an increase in the value of fracture strain from $\varepsilon_{1f}/\sqrt{3}$ for plane strain to ε_{1f} for plane stress. This would lead to an estimated maximum toughness enhancement of $\sqrt{3}$ for complete delamination within the process zone, as shown in Figure 8. In most cases, specimens which have exhibited crack divider delamination have shown fracture toughness enhancement

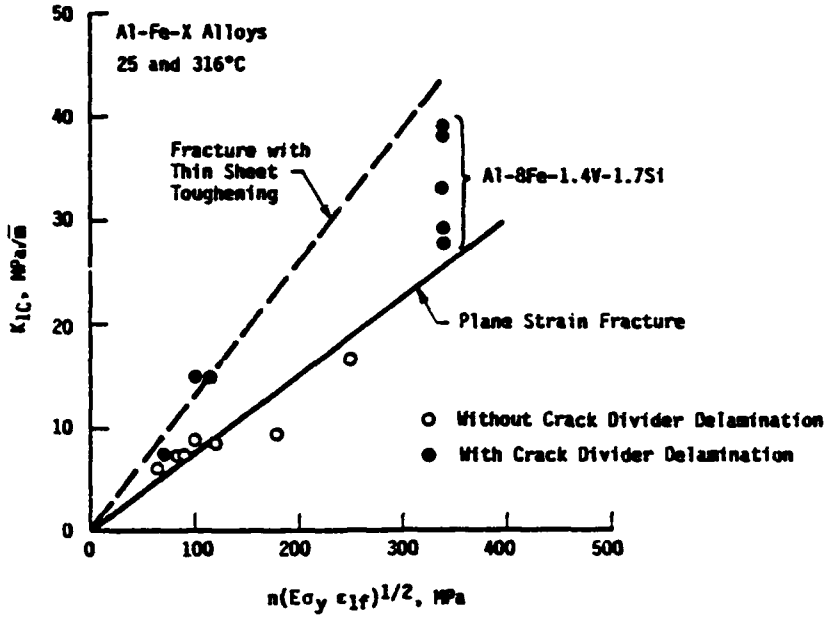

Figure 7. Comparison of calculated experimental K_{IC} results as a function of $n\sqrt{E\sigma_y\varepsilon_{1f}}$. The dash line is the model prediction for fracture with thin sheet toughening, while the solid line, which is fitted to results of the Al-Fe-Ce, Al-Fe-V, and Al-Fe-Mo-V alloys at 25°C, is the model calculation for plane strain fracture.

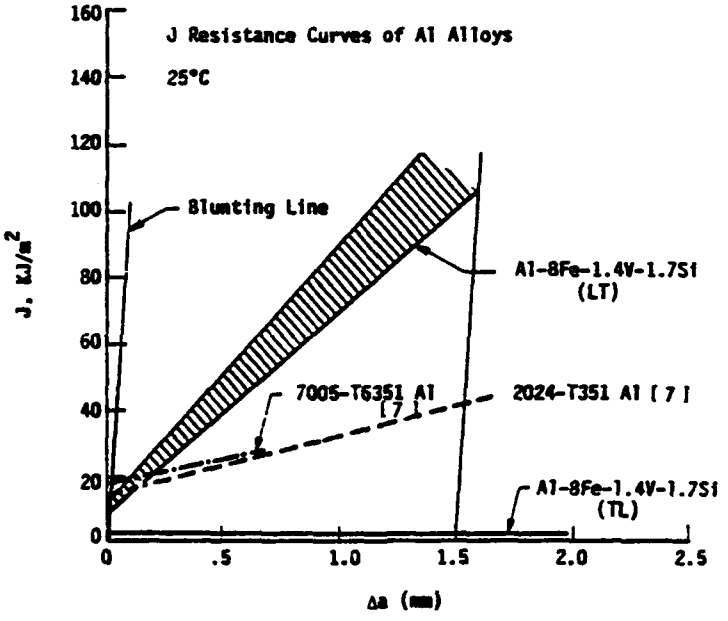

Figure 8. Comparison of the J-resistance curves of Al-8Fe-1.4V-1.7Si with those of two conventional Al-alloys.

approaching the $\sqrt{3}$ maximum limit. The wide range of fracture toughness values observed in the Al-Fe-V-Si alloys was a reflection of differences in the extent of internal delamination and thin sheet toughening present in individual specimens.

5. Discussion on Toughness Enhancement

Based on the results of the last three years, it can be concluded that high fracture toughness in Al-Fe-X alloys can be achieved as follows : (1) elimination of large, extraneous particles, such as Al-Fe intermetallics and stringer inclusions from the microstructure; (2) reduction of dispersoid size to less than 0.01 μm diameter to increase the void nucleation strain; (3) strengthening of the matrix with coherent dispersoids; (4) manipulation of the microstructure to induce thin sheet toughening. This can be achieved by controlling prior powder particle or splat boundary strength through thermomechanical processing techniques; the latter will redistribute the broken oxide fragments to some preferred and beneficial orientation (thickness direction) to maximize thin sheet toughening in the LT orientation, but at the expense of transverse strength and fracture properties. Figure 8 compares the J-resistance curves of the Al-Fe-V-Si alloy with two conventional Al-alloys. The Al-Fe-V-Si exhibits a higher crack growth resistance in the LT orientation, but a lower one in the TL, when compared to that exhibited by conventional Al-alloys. The transverse fracture properties of state-of-the-art Al-Fe-X alloys are controlled by oxide fragments at PPBs. A possible area for improvement would be to increase both the crack initiation and propagation toughness of Al-Fe-X alloys in the transverse direction. One means to achieve this would be to increase the degassing temperature to reduce the amount of oxide fragments present in the microstructure although this also might lead to dispersoid coarsening. Thus, an optimization process may be required to obtain the desired combination of longitudinal and transverse mechanical (strength and fracture) properties.

C. Accomplishments

1. The relevant fracture mechanisms in state-of the-art Al-Fe-X alloys were identified. They included void nucleation at dispersoids and at oxide fragments located along prior powder particle boundaries.

2. High toughness in state-of-the-art Al-Fe-X alloys was shown to originate from small dispersoids with coherent interfaces, hence high resistance to void nucleation, and from thin sheet toughening resulting from crack divider delamination in the process zone.

3. Void nucleation at dispersoids was shown to occur by a localized shear process in some of the Al-Fe-X alloys, while void nucleation at oxide fragments was shown to occur by a normal stress process.

4. The origin of the brittle-to-ductile fracture transition was identified and related to the tearing modulus. A fundamental relation was developed for predicting the tearing modulus in terms of tensile properties. A general scheme for predicting brittle fracture was also developed.

5. A toughening mechanism, dubbed thin sheet toughening, was proposed for explaining the beneficial effects of crack divider delamination on fracture toughness. The proposed toughening mechanism was confirmed by critical experiments.

6. The near-tip strain and displacement fields were determined for stationary and growing cracks in Al-Fe-X alloys. The results confirmed the dominance of the HHR singularity at a stationary crack tip and the dominance of the logarithmic singularity for a growing crack. The critical condition required for the transition of the HRR singularity to the logarithmic singularity when a stationary crack extends was identified.

7. Fracture toughness values of Al-Fe-X alloys were related to the microstructure. Potential means for improving the fracture toughness of Al-Fe-X alloys were suggested.

REFERENCES

1. "Confirmation of a Thin Sheet Toughening Mechanism and Anisotropic Fracture in Al-Fe-X Alloys," by K. S. Chan, **Met. Transaction A.**, 1989 (in press).

2. "Fracture Mechanisms in Al-Fe-X Alloys," K. S. Chan, **Dispersion Strengthened Aluminum Alloys**, edited by Y.-W. Kim and W. M. Griffith, TMS, Warrendale, PA, 1988, pp. 283-308.

3. "Evidence of a Thin Sheet Toughening Mechanism in Al-Fe-X Alloys," K. S. Chan, **Met. Transaction A.**, Vol. 20A, 1989, pp. 155-164.

4. H. C. Rogers, **Act. Met.**, Vol. 7, 1959, p. 750.

5. J. Q. Clayton and J. F. Knott, **Metal Sciences, 1976**, Vol. 10, 1976, p. 63.

6. "A New Criterion for Brittle-To-Ductile Fracture Transition," K. S. Chan, **Acta Metallurgica**, 1989, (in press).

7. C. A. Griffis and G. R. Yoder, **Trans. ASME, J. Eng. Mat. and Tech.**, Vol. 98, 1976, pp. 152-158.

8. A. K. Vasudevan and S. Suresh, **Mat. Sci. and Eng.**, Vol. 72, 1985, pp. 37-49.

9. S. Suresh, A. K. Vasudevan, M. Tosten, and P. R. Howell, **Acta Met.**, Vol. 35, 1987, pp. 25-46.

10. "Crack Tip Behaviors of Stationary and Growing Cracks in Al-Fe-X Alloys: Part I - Near-Tip Strain Field," K. S. Chan, **Met. Trans. A**, 1989 (submitted).

11. "Crack Tip Behaviors of Stationary and Growing Cracks in Al-Fe-X Alloys: Part II - Crack Opening Profile," K. S. Chan, **Met. Trans. A**, 1989 (submitted).

12. R. C. Dorward, **Scripta Met.**, Vol. 20, 1986, pp. 1375-1383.

13. K. T. Venkateswara Rao, W. Wu, and R. O. Ritchie, **Met. Trans.**, 1989, (in press).

14. R. H. Van Stone, R. H. Merchant, and J. R. Low, in **Fatigue and Fracture Toughness--Cryogenic Behavior**, ASTM STP 556, ASTM, Philadelphia, 1974, p. 93.

15. J. R. Rice and M. A. Johnson, in **Inelastic Behavior of Solids**, edited by M. F. Kanninen, W. F. Adler, A. R. Rosenfield, and R. I. Jaffee, McGraw-Hill, N.Y., p. 641.

16. D. Y. Lee and D. E. Zupon, in **Dispersion Strengthened Aluminum Alloys**, edited by Y.-W. Kim and W. M. Griffith, TMS, Warrendale, PA, 1988, pp. 265-281.

III. LIST OF PUBLICATIONS

Task I. Crack Tip Micromechanics and Fatigue Lifetime Prediction

1. "The Distribution of Strain within Crack Tip Plastic Zones," D. L. Davidson, ***Engineering Fracture Mechanics 25,*** 1986, pp. 123-132.

2. "The Breakdown of Crack Tip Microstructure During Fatigue Crack Extension," D. L. Davidson and J. Lankford in **High Strength Powder Metallurgy Aluminum Alloys - II**, G. J. Hildeman and M. J. Koczak, eds., TMS-AIME, Warrenville, PA, 1986, pp. 47-59.

3. "Plasticity Induced Fatigue Crack Closure," D. L. Davidson, ASTM-STP 982, **Mechanics of Fatigue Crack Closure**, J. C. Newman and W. Elber, eds., ASTM, Philadelphia, 1988, pp. 44-61.

4. "The Dependence of Crack Closure on Fatigue Loading Variables," S. J. Hudak and D. L. Davidson, ibid., pp. 121-138.

5. "Microstructural and Fatigue Crack Tip Characterization of CORONA-5 and Powder Metallurgy Ti-6Al-4V," D. L. Davidson, D. Eylon and F. H. Froes, in **Microstructure, Fracture Toughness and Fatigue Crack Growth Rate in Titanium Alloys**, A. K. Chakrabarti and J. C. Chesnutt, eds., TMS-AIME, Warrenville, PA, 1987, pp. 19-37.

6. "The Micromechanisms of Small Fatigue Crack Growth and the Influence of Metallurgical Factors," J. Lankford and D. L. Davidson, ***Fatigue '87***, EMAS Cradley Heath, UK, 1988, pp. 1769-1798.

7. "Small and Large Fatigue Cracks in Aluminum Alloys," D. L. Davidson, ***Acta Metallurgica***, V. 36, 1988, pp. 2275-2282.

8. "Determination of the Local Driving Force for Fatigue Crack Growth and a Variable Amplitude Loading, D. L. Davidson, in **Fatigue Crack Growth Under Variable Amplitude Loading**, J. Petit, D. L. Davidson, S. Suresh and P. Rabbe, eds., Elsevier Applied Science, London, 1988, pp. 1-11.

9. "The Initiation and Growth of Fatigue Cracks in a Titanium Aluminide Alloys," D. L. Davidson, J. B. Campbell and R. A. Page, AFOSR Special Technical Report, April 1988, pp. 1-52.

Task II. Microstructural/Property Relationships in Advanced Structural Alloys

1. "Fracture Mechanisms in Al-Fe-X Alloys," K. S. Chan, **Dispersion Strengthened Aluminum Alloys**, edited by Y.-W. Kim and W. M. Griffith, TMS, Warrendale, PA, 1988, pp. 283-308.

2. "Evidence of a Thin Sheet Toughening Mechanism in Al-Fe-X Alloys," K. S. Chan, ***Met. Transaction A.***, Vol. 20A, 1989, pp. 155-164.

3. "A New Criterion for Brittle-To-Ductile Fracture Transition," K. S. Chan, ***Acta Metallurgica***, 1989 (in press).

4. "Confirmation of a Thin Sheet Toughening Mechanism and Anisotropic Fracture in Al-Fe-X Alloys," by K. S. Chan, ***Met. Transaction A.***, 1989 (in press).

5. "Crack Tip Behaviors of Stationary and Growing Cracks in Al-Fe-X Alloys: Part I: Near-Tip Strain Field," K. S. Chan, ***Met. Trans. A.***, 1989 (submitted).

6. "Crack Tip Behaviors of Stationary and Growing Cracks in Al-Fe-X Alloys: Part II: Crack Opening Profile," K. S. Chan, ***Met. Trans. A.***, 1989 (submitted)

7. "Effects of Interfacial Strength on Fatigue Crack Growth in a Fiber-Reinforced Ti-Alloy Composite," by K. S. Chan and D. L. Davidson, submitted to ***Met. Trans.***, 1989.

IV. PROGRAM PERSONNEL

Name	Title	
Dr. James Lankford	Institute Scientist	Co-Principal Investigators
Dr. David L. Davidson	Institute Scientist	
Dr. Gerald R. Leverant	Director, Materials Sciences	
Dr. Kwai S. Chan	Principal Engineer	
Mr. John Campbell	Senior Technician	
Mr. Tom Masden	Senior Technician	
Mr. James Spencer	Senior Technician	
Mr. Kyle Short	Senior Technician	